Modelling magnetic fields in the corona using nonlinear force-free fields

M. S. Wheatland[1*] and K. D. Leka[2]

[1]*Sydney Institute for Astronomy, School of Physics, The University of Sydney, NSW 2006, Australia*
[2]*North West Research Associates, Colorado Research Associates Division, Boulder CO, USA*

Abstract. Force-free magnetic fields, in which the magnetic or Lorentz force is self-balancing and hence zero, provide a simple model for fields in the Sun's corona. In principle the model may be solved using boundary values of the field derived from observations, e.g. data from the Hinode spectro-polarimeter. In practise the boundary data is inconsistent with the model, because fields at the photospheric level are subject to non-magnetic forces, and because of substantial uncertainties in the boundary data. The 'self-consistency' procedure (Wheatland & Régnier 2009) provides an approach to resolving the problem. This talk reports on results achieved with the procedure, in particular new results obtained for active region AR 10953 using Hinode data incorporating uncertainties in the boundary conditions (Wheatland & Leka 2011).

Keywords : Sun: magnetic topology – Sun: corona – methods: numerical

1. Introduction

Sunspot magnetic fields power large-scale solar activity, including solar flares and Coronal Mass Ejections, and the space weather effects of these events motivate modelling of the source fields at the Sun (Committee On The Societal & Economic Impacts Of Severe Space Events 2008). Modern society is increasingly dependent on space-based communication systems. These may be damaged during severe space weather events, potentially incurring large economic losses (Odenwald, Green & Taylor 2006).

'Vector magnetograms' are maps of the magnetic field vector **B** over regions on

---

*email: michael.wheatland@sydney.edu.au

the Sun's photosphere, derived from spectro-polarimetric measurements of photo-spheric lines showing the Zeeman effect. As Del Toro Iniesta & Cobo (1996) emphasized, "nobody can measure physical quantities of the solar atmosphere" – vector magnetograms represent an *inference* of the magnetic field at the photosphere, but are not direct measurements. The 'Stokes inversion' procedures used to derive vector magnetogram field values are method and model dependent (Del Toro Iniesta 2003). Additional uncertainty is introduced by the need to resolve the intrinsic 180-degree ambiguity in the direction of the field transverse to the line of sight (Metcalf et al. 2006; Leka et al. 2009). Subject to these substantial uncertainties, vector magnetograms provide photospheric values $\mathbf{B} = (B_x, B_y, B_z)$ of the magnetic field in local heliospheric coordinates x, y, z (with z radially out). It is common to neglect the curvature of the Sun on the active region scale.

In principle, vector magnetogram data are boundary conditions for coronal field modeling (often called 'reconstruction' or 'extrapolation'), and a new generation of instruments is providing high quality data, including the space-based Hinode Solar Optical Telescope Spectro-Polarimeter (SOT/SP) (Tsuneta et al. 2008), and the Solar Dynamics Observatory Helioseismic & Magnetic Imager (SDO/HMI) (Scherrer, Hoeksema & The HMI Team 2006).

A popular model for the coronal magnetic field is the force-free model:[1]

$$\mathbf{J} \times \mathbf{B} = 0 \quad \text{and} \quad \nabla \cdot \mathbf{B} = 0, \tag{1}$$

where $\mathbf{J} = \mu_0^{-1} \nabla \times \mathbf{B}$ is electric currrent density. Physically this represents a static magneto-hydrodynamic model in which the Lorentz force dominates over other forces, and hence is zero in static equilibrium, i.e. $\mathbf{J}$ is parallel to $\mathbf{B}$. Eqns. 1 may be rewritten as

$$\mathbf{B} \cdot \nabla \alpha = 0 \quad \text{and} \quad \nabla \times \mathbf{B} = \alpha \mathbf{B} \tag{2}$$

introducing the force-free parameter α defined by $\mathbf{J} = \alpha \mathbf{B} / \mu_0$. The boundary conditions on the model in a half space ($z > 0$) are B_z over $z = 0$ together with α over $z = 0$ in the region where $B_z > 0$ (the 'P polarity'), *or* in the region where $B_z < 0$ (the 'N polarity') (Grad & Rubin 1958). There is a choice for the boundary conditions on α because this parameter is constant along magnetic field lines, according to the first of Eqns. 2.

Vector magnetograms provide two sets of boundary conditions at the photosphere (the $z = 0$ plane): B_z is provided, and α may be constructed over both the P and N regions, using the vertical electric current density J_z estimated from the vector magnetogram field values:

$$\mu_0 J_z|_{z=0} = \left. \frac{\partial B_y}{\partial x} \right|_{z=0} - \left. \frac{\partial B_x}{\partial y} \right|_{z=0}, \tag{3}$$

---

[1]In this paper, by 'model' we mean the force-free model, and by 'solution' we mean a specific solution to that model.

together with $\alpha = \mu_0 J_z / B_z$. Hence in principle there are two solutions (the *P* and *N* solutions) to the force-free model for vector magnetogram boundary data. The *P* solution uses the boundary values of B_z over the entire magnetogram, and the α values over the *P* polarity. The *N* solution uses the boundary values of B_z over the entire magnetogram, and the α values over the *N* polarity. If the boundary conditions are consistent with the force-free model, the two solutions will match. In practise the solutions do not match, and in particular they have different field line structures and magnetic energies (Metcalf et al. 2008; Schrijver et al. 2008). This is the 'inconsistency' problem.

Fig. 1 illustrates the problem: it shows the *P* solution in panel (a) and the *N* solution in panel (b) for Hinode-derived vector magnetogram boundary data for active region AR 10953, observed on 30 April 2007. The solutions were calculated with a code implementing a Grad-Rubin (1958) method of solution of Eqns. 2 (Wheatland 2007). The field lines are shown in the figure by the curved structures in the panels, and the photospheric values of B_z are shown by the greyscale image in the background. The field lines are quite dissimilar, with the *N* solution being much more distorted than the *P* solution, due to the presence of larger electric currents densities $J_z = \alpha B_z$ in the boundary values. The energies of the two solutions are also shown: the *P* solution has energy $E = 1.03 E_0$, and the *N* solution has energy $E = 1.15 E_0$, where E_0 is the energy of the potential (current-free) field with the same boundary values of B_z.

The inconsistency problem occurs because the solar atmosphere is not force free at the height of the vector magnetogram field determinations (Metcalf et al. 1995), and also because of the substantial uncertainties in the inferred field values. Inconsistency renders force-free modeling from vector magnetogram data unreliable (De Rosa et al. 2009). The procedure of 'preprocessing' (Wiegelmann, Inhester & Sakurai 2006) which is sometimes applied to vector magnetogram data before reconstruction *does not solve the problem.* Preprocessed boundary data remain inconsistent with the force-free model. Similarly, non Grad-Rubin methods of solving the force-free equations such as optimization (Wheatland, Sturrock & Roumeliotis 2000), which use the vector field **B** at the photosphere as boundary conditions and hence arrive at a single 'solution,' *do not solve the inconsistency problem* – the solution must depart from the force-free model, and hence is inaccurate and unreliable. Nonlinear force-free modeling from vector magnetogram boundary data *should not be trusted for quantitative analysis and interpretation of the Sun's coronal magnetic field.*

2. The self-consistency procedure

The 'self-consistency procedure' (Wheatland & Régnier 2009) provides one approach to the problem of the mismatch between vector magnetogram boundary data and the force-free model. The idea is to find a solution to the force-free model which is 'close' to matching the vector magnetogram boundary data on α for both the *P* and the *N*
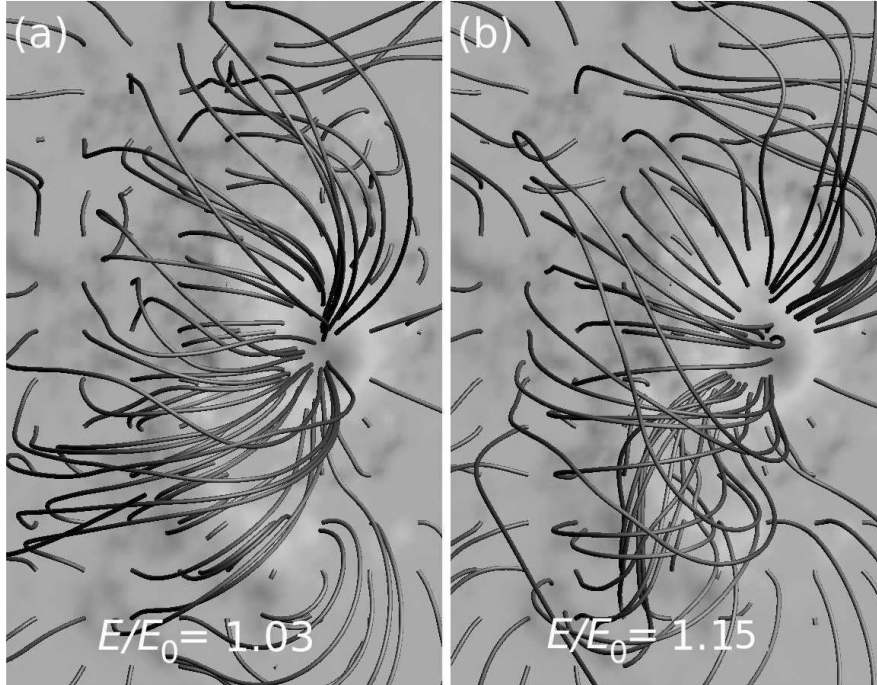
Figure 1. The two inconsistent nonlinear force-free solutions for vector magnetogram boundary conditions for AR 10953: (a) the *P* solution; (b) the *N* solution.

solutions. A similar, but different scheme has recently been presented by Amari & Aly (2010).

The procedure may be summarised in three steps. At step one, *P* and *N* solutions are constructed, using the Grad-Rubin procedure, from the vector magnetogram boundary data. At step two, the boundary conditions on α are adjusted, based on the solutions and uncertainties in the boundary values of α. Specifically, the *P* and *N* solutions define two sets of α values at $z = 0$: $\alpha_P \pm \sigma_P$ and $\alpha_N \pm \sigma_N$ (each of which is consistent with the force-free model). Bayesian probability (Jaynes & Bretthorst 2003) is used to estimate 'true' values for α, under the assumption that these are two sets of observations of the same data with Gaussian uncertainties. The estimates are (Wheatland & Régnier 2009):

$$\alpha_{\rm est} = \sigma_{\rm est}^2 \left(\alpha_P/\sigma_P^2 + \alpha_N/\sigma_N^2 \right) \quad \text{with} \quad \sigma_{\rm est}^2 = \frac{1}{1/\sigma_P^2 + 1/\sigma_N^2}. \tag{4}$$

The $\alpha_{\rm est}$ values are still inconsistent with the force-free model, but are expected to be closer to consistency. Step three in the procedure is to iterate steps one and two until consistency is achieved, i.e. until the *P* and *N* solutions (and their boundary values) match. At each iteration, the vector magnetogram boundary values of α used in step

one are replaced by the new estimates $\alpha_{\text{est}} \pm \sigma_{\text{est}}$. The iterations of the procedure are called 'self-consistency cycles.'

The self-consistency procedure was initially tested on Hinode SOT/SP data for active region AR 10953 on 30 April 2007 (see Fig. 1), in Wheatland & Régnier (2009). This region was the subject of nonlinear force-free modeling using a number of different nonlinear force-free solution codes in an earlier study (De Rosa et al. 2009), which highlighted the many difficulties associated with the modeling, in particular the consistency problem. The self-consistency modeling of AR 10953 presented in Wheatland & Régnier (2009) demonstrated that the method works in application to vector magnetogram data: a self-consistent solution was obtained. However, the results were considered to be a 'proof of concept,' rather than a realistic solution for the coronal field because different uncertainties σ were not assigned to the different boundary values of α (all boundary points were assumed to have equal values of σ). This neglect resulted in a self-consistent solution that was close to potential: the energy of the final field was $E/E_0 = 1.02$. Recently the calculation was repeated, including uncertainties derived from the Stokes inversion procedure used to construct the vector magnetogram (Wheatland & Leka 2011). The inclusion of different uncertainties at different boundary points acts to preserve boundary values of α at points where σ is small, i.e. where the boundary values are well-determined. This follows from the uncertainty-weighted averaging in Eqns. 4. The boundary values of α tend to be more certain where the field is stronger (e.g. in the core of an active region), and these locations tend to include large electric currents. The corresponding large values of $J_z = \alpha B_z$ are preserved over the self-consistency cycles, leading to more significant departure from the potential field configuration (by comparison with the case when the individual uncertainties are ignored).

In the following section we briefly summarise the new results for the modeling of active region AR 10953, including uncertainties, as presented in detail in Wheatland & Leka (2011).

3. Modeling AR 10953 with uncertainties

In the revised modeling of active region AR 10953 (Wheatland & Leka 2011), the initial data consists of an Hinode SOT/SP vector magnetogram merged with Solar and Heliospheric Observer Michelson Doppler Interferometer (SoHO/MDI) line-of-sight magnetic field data (Scherrer et al. 1995). The merging provides boundary data over a wider field of view at the photosphere than is provided by Hinode observations alone. The data grid is of size 313×313 with a grid spacing of 0.8 arcseconds. The Hinode Stokes inversion process involves nonlinear least-squares fitting of a model atmospheric spectrum to the observed spectrum, for each set of observed Stokes profiles. This gives magnetic field values with uncertainties, where the uncertainties are based on the χ^2 values of the goodness of fit. These uncertainties are considered to be lower bounds to more realistic uncertainties because they involve only the curvature

of the fit in the χ^2 space, and neglect e.g. systematic errors, photon noise, and the question of the validity of the atmospheric modeling. The resulting Hinode SOT/SP boundary field values with uncertainties are converted into boundary values $\alpha \pm \sigma$ for the force-free parameter using Eqn. 3 together with propagation of uncertainties. Boundary points in the MDI data region are assigned $\alpha = 0$ and a large (nominal) uncertainty.

The Wheatland (2007) nonlinear force-free code is used to calculate solutions on a $313 \times 313 \times 300$ grid, from the Hinode/MDI vector magnetogram boundary conditions. The Grad & Rubin (1958) method used by the code involves iterative solution of a set of linear partial differential equations, such that the iteration sequence is expected to converge to a solution to the nonlinear system of Eqns. 2. At each self-consistency cycle, $N_{\mathrm{GR}} = 30$ Grad-Rubin iterations are used to construct individual P and N solutions, and this process is repeated over a chosen number of self-consistency cycles. The self-consistency procedure is found to converge in less than 10 cycles. The energies of the final P and N solutions are both $E/E_0 = 1.08$, with the two solutions differing in energy by $< 0.03\%$. The energy is intermediate between the energies of the initial P and N solutions (see Fig. 1).

Fig. 2 shows the self-consistent solutions obtained, with the same display as that used in Fig. 1. Panel (a) shows the P solution and panel (b) shows the N solution. The field lines for the two solutions are very similar, illustrating the achievement of self-consistency. The field is quite distorted, indicating substantial non-potentiality. The inclusion of individual uncertainties in the boundary conditions on electric current density has resulted in the preservation of well-determined large currents, leading to larger energy, by comparison with the earlier calculation presented in Wheatland & Régnier (2009).

The self-consistency procedure alters the boundary values of α (and hence of $J_z = \alpha B_z$) but does not alter the boundary values of B_z. When individual uncertainties σ are assigned to the α values, the values tend to be preserved at locations with small values of σ. Inspection of the distribution of J_z at the photosphere for the vector magnetogram and the self-consistent solution shows that, while the details vary, structures in the current with a large signal-to-noise ratio are preserved. Quantitatively, the individual values are altered substantially, leading to relatively large changes in the horizontal field components B_x and B_y. Fig. 3 shows histograms of $\Delta B_h = \left[(B_x^f - B_x^i)^2 + (B_y^f - B_y^i)^2 \right]^{1/2}$, where i denotes values in the initial vector magnetogram, and f the self-consistent solution, for the same boundary points. Only points in the Hinode data region are included. The average absolute change in the horizontal field is $\langle \Delta B_h \rangle \approx 170\,\mathrm{Mx/cm}^2$, and the average change in units of the uncertainties is $\langle \Delta B_h / \sigma_{B_h} \rangle \approx 9$. Many points are subject to a change substantially larger than the corresponding uncertainty. As discussed in Section 3, these uncertainties may be interpreted as lower bounds. In addition, the data is expected not to be force-free, i.e. to vary by more than the uncertainties with respect to force-free boundary data.
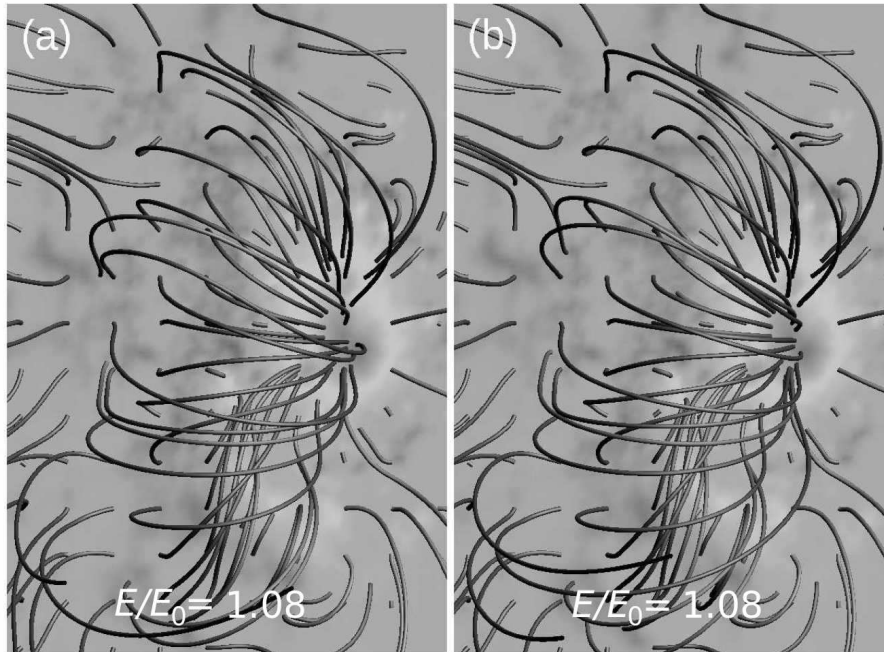
Figure 2. The self-consistent nonlinear force-free solutions obtained for AR 10953: (a) the *P* solution; (b) the *N* solution.

Another problem with nonlinear force-free modeling, related also to inconsistency, is that the iterative methods used to solve the nonlinear force-free model tend not to converge, strictly, when applied to solar vector magnetic field data (Schrijver et al. 2008; De Rosa et al. 2009). The Grad-Rubin procedure exhibits slow oscillations in field structures and energy rather than converging to a static field with a fixed energy. This is due to the presence of large localised values of $J_z = \alpha B_z$ in the boundary conditions. Because of this the *P* and *N* solutions constructed at early self-consistency cycles depend in detail on the choice of the number N_{GR} of Grad-Rubin iterations used. To investigate the influence of this problem on the self-consistency results, the calculation is repeated with $N_{GR} = 20$ and $N_{GR} = 40$ iterations at each cycle. In each case the results are very similar to those obtained with $N_{GR} = 30$ Grad-Rubin iterations, and in particular the new energies are all found to be $E/E_0 = 1.08$, to the stated digits. This suggests that the final results are robust despite the early dependence of the calculations on this parameter.

4.   Conclusions

Accurate modeling of magnetic fields in the Sun's corona is needed to better understand various processes including the origins of space weather events. In principle
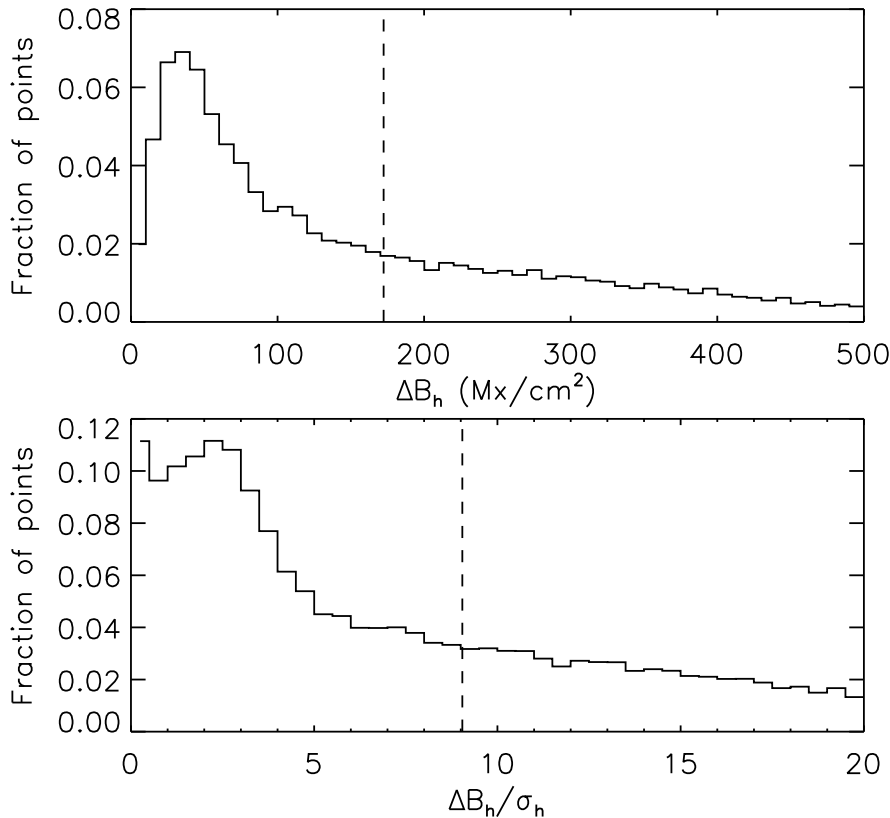
Figure 3. Quantitative changes ΔB_h in the horizontal field at the photosphere produced by the self-consistency procedure. The change is defined as $\Delta B_h = \left[(B_x^f - B_x^i)^2 + (B_y^f - B_y^i)^2 \right]^{1/2}$, with i denoting values in the initial vector magnetogram, and f the final values in the self-consistent solution. Upper panel: histogram of changes in absolute values. Lower panel: the changes in units of the uncertainties. The vertical dashed lines indicate the average values.

vector magnetograms (maps of the inferred magnetic field at the photosphere) provide boundary conditions for modeling the corona using the nonlinear force-free model. In practise vector magnetogram boundary data are inconsistent with the nonlinear force-free model, and the modeling is unreliable (Schrijver et al. 2008; De Rosa et al. 2009). This point does not seem to be widely appreciated, so it is worth restating, in dramatic terms: nonlinear force-free modeling from vector magnetogram boundary data *should not be trusted!*

An approach to solving this problem – the self-consistency procedure – is explained. The method has been demonstrated in application to Hinode SOT/SP data for active region AR 10953 (Wheatland & Régnier 2009). The original calculation

neglected individual uncertainties in the boundary conditions on electric current density, which led to the self-consistent solution being close to potential (current-free), with a relatively small magnetic energy ($E/E_0 = 1.02$, where E_0 is the energy of the potential field with the same boundary conditions on B_z). Recently the calculation was revisited with individual uncertainties included (Wheatland & Leka 2011). This is an important new step because the uncertainties act to preserve the electric current density at locations where it is well-determined, based on the vector magnetic field data.

The new calculation is summarised here. The self-consistent solution obtained is significantly non-potential (magnetic energy $E/E_0 = 1.08$). The boundary conditions on the electric current density are substantially altered, but basic structures in the currents are preserved.

Self-consistency is a promising method for coronal magnetic field modeling. It overcomes the inconsistency problem and provides an accurate solution to the nonlinear force-free model. We emphasize again that this is not possible with nonlinear force-free methods applied directly to vector magnetogram data: either two solutions to the force-free model are obtained, or a single, inaccurate solution results. Hence the self-consistency approach makes nonlinear force-free modeling of coronal magnetic fields possible, for the first time. However, the results of the method require independent verification as an accurate representation of the magnetic field in the corona. Also, it is important to consider more physically based modeling, incorporating non-magnetic forces into the model. These topics will be examined in future studies.

Acknowledgements

References

Amari T., Aly J.-J., 2010, A&A, 522, A52

Committee On The Societal and Economic Impacts Of Severe Space Weather Events 2008, Severe Space Weather Events: Understanding Societal and Economic Impacts Workshop Report, Space Studies Board ad hoc Committee: A Workshop, The National Academies Press: Washington, DC ISBN: 978-0-309-12769-1

De Rosa M. L., et al., 2009, ApJ, 696, 1780

Del Toro Iniesta J. C., 2003, Introduction to Spectropolarimetry, Cambridge University Press: Cambridge, UK ISBN: 0521818273

Del Toro Iniesta J. C., Ruiz Cobo B., 1996, Solar Phys., 164, 169

Grad H., Rubin H., 1958, in Proc. 2nd Int. Conf. on Peaceful Uses of Atomic Energy, Vol. 31, Geneva: UN, 190

Jaynes E. T., Bretthorst G. L., 2003, Probability Theory, Cambridge University Press: Cambridge, UK ISBN 0521592712

Leka K. D., Barnes G., Crouch A. D., Metcalf T. R., Gary G. A., Jing J., Liu Y., 2009, Solar Phys., 260, 83

Metcalf T. R., Jiao L., McClymont A. N., Canfield R. C., Uitenbroek H., 1995, ApJ, 439, 474

Metcalf T. R., et al., 2006, Solar Phys., 237, 267

Metcalf T. R., et al., 2008, Solar Phys., 247, 269

Odenwald S., Green J., Taylor W., 2006, AdSpR, 38, 280

Scherrer P. H., et al., 1995, Solar Phys., 162, 129

Scherrer P. H., Hoeksema J. T., The HMI Team, 2006, cosp, 36, 1469

Schrijver C. J., et al., 2008, ApJ, 675, 1637

Tsuneta S., et al., 2008, Solar Phys., 249, 167

Wheatland M. S., 2007, Solar Phys., 245, 251

Wheatland M. S., Leka K. D., 2011, ApJ, 728, 112

Wheatland M. S., Régnier S., 2009, ApJ, 700, L88

Wheatland M. S., Sturrock P. A., Roumeliotis G., 2000, ApJ, 540, 1150

Wiegelmann T., Inhester B., Sakurai T., 2006, Solar Phys., 233, 215